

# Lawrence Berkeley National Laboratory

## Lawrence Berkeley National Laboratory

### **Title**

Three dimensional interpretations of single-well electromagnetic data for geothermal applications

### **Permalink**

<https://escholarship.org/uc/item/5db1478g>

### **Authors**

Tseng, Hung-Wen  
Lee, Ki Ha

### **Publication Date**

2004-01-09

## THREE DIMENSIONAL INTERPRETATIONS OF SINGLE-WELL ELECTROMAGNETIC DATA FOR GEOTHERMAL APPLICATIONS

Hung-Wen Tseng<sup>1</sup>, and Ki Ha Lee<sup>2</sup>

Earth Sciences Division  
Lawrence Berkeley National Laboratory  
1 Cyclotron Road  
Berkeley, CA 94720

1. e-mail: [hwtseng@lbl.gov](mailto:hwtseng@lbl.gov)
2. e-mail: [khlee@lbl.gov](mailto:khlee@lbl.gov)

### **ABSTRACT**

An efficient 3-D electromagnetic (EM) inversion algorithm has been developed for geothermal applications and tested successfully using a set of single-hole EM logging data. The data was collected at an oil field undergoing CO<sub>2</sub> injection in southern California using a single-hole EM tool, Geo-BILT, developed by Electromagnetic Instruments, Inc (EMI). The tool is equipped with a multi-component source, and multi-component receivers at different separations. The inversion result provides a reasonable electrical conductivity image to a distance of 10 m from the well, and illustrates several zones with lateral conductivity variations that could not be resolved with traditional induction logging tools. The successful case study demonstrates potential applications of the tool and software for characterizing fracture systems in geothermal reservoirs.

### **INTRODUCTION**

Electrical conductivity is related to the porosity, pore fluid conductivity, saturation, temperature, and clay content of rocks. This intrinsic relationship justifies the use of EM geophysical methods with applications to geohydrology, enhanced oil recovery monitoring, engineering geophysics, monitoring of environmental remediation processes, and geothermal exploration. Traditionally, EM induction logging is widely used for directly measuring the formation conductivity surrounding uncased wells. Such logging tools primarily consist of a magnetic dipole transmitter and a receiver in a coaxial configuration in line with the borehole axis. As a result of this cylindrically symmetric nature of the source and receiver, induction logging data offers no information about the 3-D conductivity distribution in the vicinity of the borehole. The 3-D conductivity structure surrounding a borehole can only be characterized if multiple components of the magnetic fields due to

various source polarizations are acquired (Alumbaugh and Wilt, 2001). Electromagnetic Instrument (EMI) has developed a single-hole induction logging system dubbed the Geo-BILT system. The tool consists of a three-component magnetic source and two three-component inductive receivers spaced at 2 and 5 meters, respectively, from the transmitter. This results in two 3x3 tensor data at two separations for a specific source depth. However, 3-D interpretations using such single-hole EM data is difficult because of the richness and complexity of the data and the very large number of discretized conductivity elements needed to represent a realistic earth model. Taking advantage of the computing efficiency of an algorithm based on a modified extended Born approximation (MEBA, Tseng et al., 2003), we developed an inversion code for interpreting EM data acquired in a single-hole environment common in geothermal areas. Following a brief description of the theory, synthetic data derived from simulating a thin sheet model is used to demonstrate the algorithm. Then data from an oil field in southern California is interpreted.

### **THE MEBA 3-D INVERSION ALGORITHM**

Based on the integral equation method (Hohmann, G. W., 1975) for geophysical EM simulations, the magnetic field,  $\mathbf{H}$ , at a location,  $\mathbf{r}_r$ , produced by an EM source can be evaluated using

$$\mathbf{H}(\mathbf{r}_r) = \mathbf{H}_b(\mathbf{r}_r) - i\omega\mu_0 \int_{V_a} \overset{=H}{\mathbf{G}}(\mathbf{r}_r, \mathbf{r}') \Delta\sigma(\mathbf{r}') \cdot \mathbf{E}(\mathbf{r}') d\mathbf{r}' \quad (1)$$

where  $\mathbf{H}_b$  is the primary magnetic field due to the source;  $\Delta\sigma$  is the conductivity anomaly in a layered subsurface;  $\mathbf{E}(\mathbf{r}')$  is the total electric field in the anomaly;  $\overset{=H}{\mathbf{G}}$  is the Green's function relating the magnetic field at  $\mathbf{r}_r$  to a current source at  $\mathbf{r}'$ ;  $\omega$  is the angular frequency, and  $\mu_0$  is the free space magnetic permeability. The electric field,  $\mathbf{E}(\mathbf{r}')$ , may be derived by solving an integral equation for a discretized model. However, the technique becomes impractical as the number of the discretized model

parameter is increased. This computational hurdle can be avoided using approximate techniques, such as the modified extended Born approximation (Tseng et al., 2003). With this approximation, the electric field in the conductivity anomaly can be calculated using

$$\mathbf{E}(\mathbf{r}') \approx \overline{\overline{\Gamma}}^m(\mathbf{r}') \cdot \mathbf{E}_b(\mathbf{r}') \quad (2)$$

where  $\overline{\overline{\Gamma}}^m$  is a 3x3 tensor expressed as:

$$\overline{\overline{\Gamma}}^m(\mathbf{r}') = \left[ \overline{\overline{\mathbf{I}}} + i\omega\mu_0\sigma(\mathbf{r}') \int_{V_s} \overline{\overline{\mathbf{G}}}^E(\mathbf{r}', \mathbf{r}'') \frac{\Delta\sigma(\mathbf{r}'')}{\sigma(\mathbf{r}'')} d\mathbf{r}'' \right]^{-1} \quad (3)$$

Here,  $\sigma$  is the conductivity;  $\overline{\overline{\mathbf{G}}}^E$  is the Green's tensor relating the electric field at  $\mathbf{r}'$  to a current source at  $\mathbf{r}''$ , and  $\overline{\overline{\mathbf{I}}}$  is a unit tensor. Application of the fast Fourier transform technique to the integral of (3) makes the MEBA code efficient for low frequency EM 3-D simulation. The MEBA code is incorporated into a 3-D non-linear inversion algorithm based on a least-squares approach following Oldenburg et al. (1993). An updated model,  $\mathbf{m}^{k+1}$ , is derived by solving the following system of equations:

$$\begin{aligned} & (\overline{\overline{\mathbf{J}}}^T \overline{\overline{\mathbf{W}}}_d^T \overline{\overline{\mathbf{W}}}_d \overline{\overline{\mathbf{J}}} + \lambda \overline{\overline{\mathbf{W}}}_m^T \overline{\overline{\mathbf{W}}}_m) \mathbf{m}^{k+1} \\ & = \overline{\overline{\mathbf{J}}}^T \overline{\overline{\mathbf{W}}}_d^T \overline{\overline{\mathbf{W}}}_d (\overline{\overline{\mathbf{J}}} \mathbf{m}^k - \mathbf{d}(\mathbf{m}^k) + \mathbf{d}^{obs}) \end{aligned} \quad (4)$$

Here, the superscript  $T$  denotes transpose of the matrix;  $k$  is the iteration number and  $\mathbf{d}(\mathbf{m}^k)$  is a column vector representing the calculated system response to the current subsurface conductivity model,  $\mathbf{m}^k$ ;  $\overline{\overline{\mathbf{W}}}_d$  is a square weighting matrix that assigns a relative importance to each data point. Usually it's a diagonal matrix with the elements equal to the inverse of the noise in the observation.

The matrix,  $\overline{\overline{\mathbf{W}}}_m$ , determines how the model is biased. In this study, a smoothness criterion based on spatial gradient is used to constrain the inversion procedure. The variable  $\lambda$  in (4) is a Lagrange multiplier that controls the degree of smoothness of the model. The Jacobian matrix,  $\overline{\overline{\mathbf{J}}}$ , which is the change in the EM field for each source-receiver pair due to the perturbation of each element of the discretized conductivity model, can be approximated based on the MEBA technique:

$$\mathbf{J}_{nj} \approx -i\omega\mu_0 \left( \overline{\overline{\Gamma}}_j^m \cdot \mathbf{E}_{b,j}^* \right) \cdot \left( \overline{\overline{\Gamma}}_j^m \cdot \mathbf{E}_{b,j} \right) \Delta V_j \quad (5)$$

Here,  $n$  is the  $n$ -th data (magnetic field),  $i$  is  $\sqrt{-1}$ ,  $\Delta V_j$  is the volume of the  $j$ -th discretized cell, and  $\mathbf{E}_{b,j}$  and  $\mathbf{E}_{b,j}^*$  are the primary electric fields in the conductivity inhomogeneity due to the real

transmitter and a fictitious source at the receiver location, respectively.

Being such a critical element for the non-linear inversions, an analysis of the Jacobian matrix is useful in understanding the sensitivity and resolving ability of a specific survey configuration. Alumbaugh and Wilt (2001) presented in detail the sensitivity functions for all of the nine possible transmitter-receiver polarizations for single-hole EM surveys. It was demonstrated that, for the co-axial transmitter-receiver configuration, the cylindrically symmetric pattern of the sensitivity function about the borehole makes 3-D structures surrounding the borehole impossible to resolve if only the co-axial data is available. Other asymmetric measurements, such as a horizontal field due to a vertical source, must be collected to obtain the 3-D conductivity structure surrounding the borehole.

For the inversion, analysis of the sensitivity matrix also helps in determining another important factor, the data-weighting matrix in (4). Due to the proximity between the source and receivers, the secondary co-axial and the co-planar data are measured in the dominant presence of the primary field due to the source. For example, assuming a vertical borehole in a 0.2 S/m whole space, at 6 kHz, the sensitivity function for a vertical magnetic dipole source and a vertical magnetic field receiver pair with a 5 m separation displayed in Figure 1(a). Here, the real and imaginary parts of the function are expressed as the logarithm of their values normalized to the corresponding maximum of the Jacobian for this configuration, with a value of  $\pm 3$  assigned at the locations where the maximum values occur and all values less than 1/1000 of the maximal assigned to 0. Both the real and imaginary parts are about the same magnitude relative to their corresponding maximum. However, if the sensitivity is normalized to the primary magnetic field, as shown in Figure 1(b), the real component is almost negligible if system noise is taken into account. In other words, only the imaginary part of the magnetic field contains significant and measurable signal that carries the information about the conductivity structure surrounding the borehole.

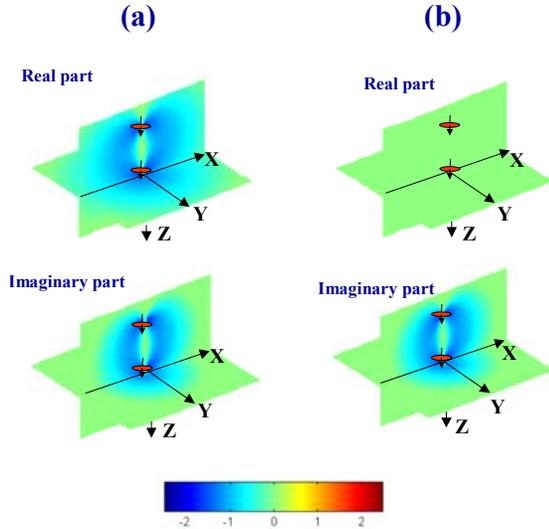


Fig. 1 Sensitivity function for a pair of co-axial transmitter-receiver configuration. (a) Logarithm of the sensitivity normalized to the maximum of the function in the whole domain. (b) Logarithm of the sensitivity normalized to the primary field calculated at the receiver.

## NUMERICAL SIMULATIONS

Originally designed for cross-hole and borehole-to-surface configurations for vertical sources and receivers only, the MEBA code has been modified for the single-hole case for any combination of the source and receiver polarizations. To verify the performance of the modified code, synthetic data from simulating a horizontal conductive plate model depicted in Figure 2 is used for inversion. Here, in a homogeneous 0.2 S/m media, the center of the square sheet, which has a dimension of 5x5x1 m and a conductivity of 1 S/m, is placed 5 m from a vertical borehole while its edges are parallel to the two horizontal coordinates, X and Y. The separation between the transmitting and the receiving units is kept at 5m and the center of the array runs from 3.5 above the level of the plate to 7.5 m below this level at 1 m intervals. An integral equation algorithm developed by Wannamaker et al. (1985) was used to compute the synthetic data at a frequency of 6 kHz.

Assuming only the vertical coaxial component,  $H_z$ , is available (Figure 3), which is the case for traditional induction logging, a cylindrically symmetric conductivity image surrounding the well at the depth of the simulated conductive plate can be obtained as illustrated in Figure 4. The location of the simulated plate is indicated by the dashed square. Though the conductivity anomaly is found at the right depth, its azimuthal distribution cannot be resolved. In addition, the value of the conductivity of the anomalous body cannot be recovered due to the smoothness criteria used to constrain the non-linear

inversion. Adding the other two orthogonal horizontal magnetic fields,  $H_x$  and  $H_y$  as shown in Figure 3, to the inversion, the depth and horizontal location of the conductive body can be clearly recovered as presented in Figure 5. However, the radial extension of the conductivity distribution derived from the inversion is still ambiguous.

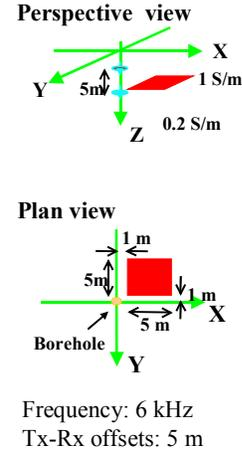


Fig. 2 A thin conductive plate model used for producing synthetic data for verifying the MEBA algorithm for single-hole EM surveys.

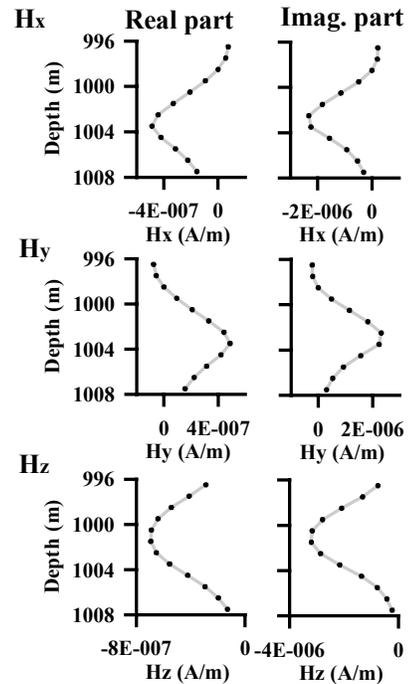


Fig. 3 Calculated magnetic fields due to a vertical magnetic source for the model presented in Figure 2.

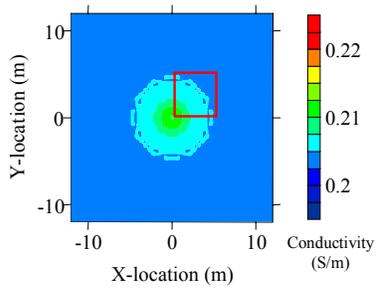


Fig. 4 Inverted conductivity on a horizontal plane at the level of the conductive plate shown in Figure 2. Only vertical magnetic field is used for inversion.

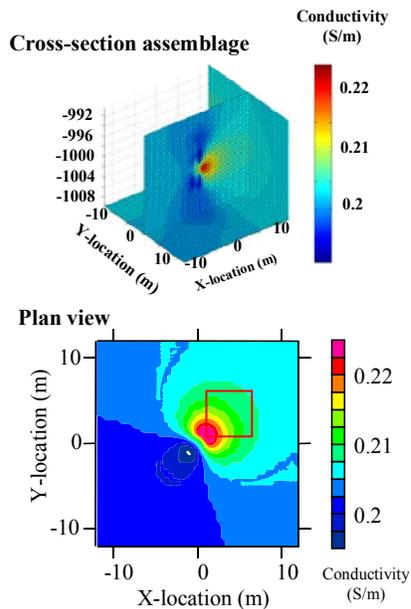


Fig. 5 Inverted conductivity on a horizontal plane at the level of the conductive plate shown in Figure 2. All the three component magnetic fields are used for inversion.

As mentioned previously, to achieve reasonable inversion results careful consideration of the weighting on the data is critical. This is particularly important in case of the co-axial data, because the primary magnetic field is dominant over the secondary field. After testing various combination of weighting coefficients for the vertical magnetic field, we decided to use the weighting on the imaginary part of the field 1000 times that for the real part. For the horizontal magnetic components, both real and imaginary parts are equally weighted since direct coupling between the vertical source and the calculated horizontal field is absent.

## THE GEO-BILT SYSTEM, FIELD DATA, AND INVERSION RESULTS

A set of single-hole data was collected by EMI with the Geo-BILT system at a Chevron oil field in southern California during a CO<sub>2</sub> pilot injection project. The area has been undergoing water flooding since 1995 for oil recovery purposes (Hoversten, et. al, 2003). Four boreholes originally used for water injection have been converted for CO<sub>2</sub> injection started in September 2000. Figure 6 displays one of the CO<sub>2</sub> injection boreholes, 11-8WR, and two fiberglass-cased wells, OB-C1 and OB-C2, used for monitoring the progress of the injection. OBC-2 was about 80 ft to the south of OBC1 and the injection well, 11-8WR, was about 20 ft, on the eastern side, off the plane including OB-C1 and OB-C2. Cross-hole EM data was collected before the commencement of the injection and a set of single-hole data was acquired in May 2001 in the well OB-C1. Only the single-hole data and its interpretation are presented here.

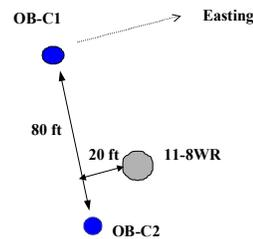


Fig. 6 Surface projection of the boreholes related to single-hole EM data collection.

From data obtained with the Geo-BILT, only the data with a vertical source and 5 m separation at 6 kHz is used for interpretation. The calibrated magnetic fields in all three coordinate directions are illustrated as the blue lines in Figure 7. Here, the center between the transmitter and the receivers is used for labeling the depth of the data. The inversion domain, between 422 to 559 m in depth, was a 21x21x137 m volume divided into 21x21x137 cells. The inversion took about 26 hours for 11 iterations using a COMPAQ Alpha workstation.

The simulation data for the final model is displayed as the red lines in Figure 7. Data mismatch for the vertical magnetic field is more obvious than the other two horizontal components. This may be due to the overwhelming dominance of the primary magnetic field over the secondary field for this component, and the real part of the field was almost neglected due to the weightings. The conductivity distribution is presented in Figure 8 in two orthogonal vertical panels centered at OB-C1: one in the north-south

direction containing the two observation boreholes (Figure 8(a)) and the other in the east-west direction (Figure 8(b)). The induction logging data in OB-C1 acquired in September 2000 is also displayed in Figure 8(d) for comparison. The conductivity structure characteristics surrounding OB-C1 matches reasonably well with the logging data. However, the results show a major lateral conductivity variation around the borehole between the depths of 507 and 525 m, which is the primary producing layer at the site. This inhomogeneity is also manifested by the relatively significant anomalies in the two horizontal magnetic fields at the same depth. The horizontal slice of the conductivity distribution at the depth of 513 m, which is illustrated in Figure 8(c), displays a trend that the conductivity is smaller on the north-east side of OB-C1 than on the south-east side of the well. This indicates that CO<sub>2</sub> has been replacing the more conductive water from the injection well, 11-8WR. Other minor lateral inhomogeneity can be observed at about 437 and 453 m, which are also apparent from the calibrated horizontal magnetic fields.

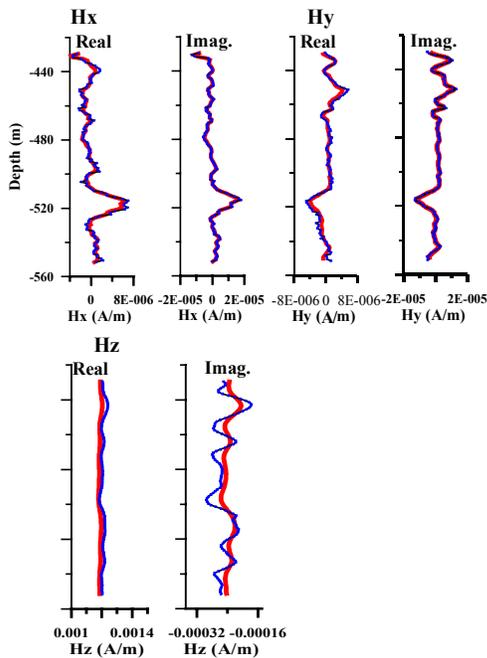


Fig. 7 Single-hole magnetic field data (in blue) in OB-C1 used for inversion. The simulation data for the inversion results are presented in red.

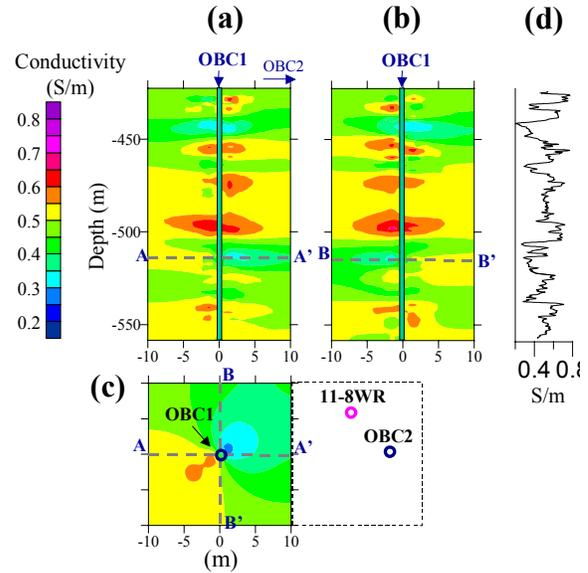


Fig. 8 Inversion results: (a) in the vertical plane containing OB-C1 and OB-C2; (b) an east-west vertical plane centered at OB-C1; and (c) horizontal slice centered at OB-C1 at the depth of 513 m. (d) Induction logging for OB-C1 at the start of the CO<sub>2</sub> injection.

## CONCLUSIONS

We have demonstrated that conductivity distribution and variation around a borehole can be obtained using EM single-hole data with an efficient 3-D inversion algorithm. Though the data we have shown was collected in an oil field undergoing oil recovery processes, the same methodology can be extended for geothermal applications. Multi-component magnetic fields, appropriate data weightings, and efficient algorithms are all required for completing the task. However, the definition of the radial extension of the inverted conductivity structure from the borehole remains ambiguous. Further studies will be necessary to alleviate this uncertainty by considering alternative model constrains, multi-frequency data, additional transmitter-receiver offsets, cross-hole, and/or surface-to-borehole configurations.

## ACKNOWLEDGEMENTS

This work was supported by the Assistant Secretary for Energy Efficiency and Renewable Energy, Office of Wind and Geothermal Technologies of the U.S. Department of Energy under Contract No. DE-AC03-76SF00098. We are also grateful for the financial support and field data offered by Electromagnetic Instrument, Inc.

## **REFERENCES**

Alumbaugh, D. L., and Wilt, M. J., 2001, A numerical sensitivity study of three dimensional imaging from a single borehole: *Petrophysics*, 42, 19-31.

Hohmann, G. W., 1975, Three-dimensional induced polarization and electromagnetic modeling: *Geophysics*, 40, 309-324.

Hoversten, G. M., Gritto, R., Washbourn, J, and Daley, T., 2003, Pressure and fluid saturation prediction in a multicomponent reservoir using combined seismic and electromagnetic imaging: *Geophysics*, 68, 1580-1591.

Oldenburg, D. W., McGillivray, R. R., and Ellis, R. G., 1993, Generalized subspace methods for large-scale inverse problems: *Geophys. J. Internat.*, 114, 12-20.

Tseng, H.-W., Lee, K. H., and Becker, A., 2003, 3D interpretation of electromagnetic data using a modified extended Born approximation: *Geophysics*, 68, 127-137.

Wannamaker, P. E., Hohmann, G. W., and San Filippo, W. A., 1984, Electromagnetic modeling of three-dimensional bodies in layered earths using integral equations: *Geophysics*, 49, 60-74.